Deciphering the role of evapotranspiration in declining relative humidity trends over land

Authors

Yeonuk Kim,[1]* Mark S. Johnson,[1,2]

Affiliations

[1] Institute for Resources, Environment and Sustainability, University of British Columbia, Vancouver, BC, Canada

[2] Department of Earth, Ocean and Atmospheric Sciences, University of British Columbia, Vancouver, BC, Canada

*Yeonuk Kim (yeonuk.kim@ubc.ca)

Abstract

In recent decades, relative humidity (*RH*) over land has declined, driving increases in droughts and wildfires. Previous explanations attribute this trend to insufficient moisture advection from the ocean to sustain *RH* over land, but this ignores atmospheric moisture supplied from terrestrial evapotranspiration (*E*). While state-of-the-art climate models underestimate this *RH* trend, the reason behind this discrepancy remains unclear. Here, we decipher the influence of *E* on near-surface humidity using observations, reanalysis, and climate simulations. Global *E* in reanalysis has remained fairly steady in recent decades. Consequently, changes in ocean advection can reproduce observed *RH* declines without considering changes in *E*. Conversely, climate simulations estimate significant increases in *E* in recent decades, leading to model-based underestimation of observed *RH* declines. These findings suggest *E* intensifications may be overestimated in current climate models, thus underestimating coupled land-atmosphere drying in model output. We also highlight an upper limit of *E* change under observed *RH* trends, which could help benchmark global *E* trend analyses.

This manuscript is a non-peer reviewed preprint submitted to EarthArXiv.

Introduction

Human-induced climate change is expected to have significant impacts on Earth's water cycle (Milly et al., 2008). Reliable predictions of future water resources require a comprehensive understanding of how climate change affects terrestrial evapotranspiration (*E*) (Fisher et al., 2017; Jung et al., 2010; Milly & Dunne, 2020), which represents the sum of evaporation from soil, intercepted water, and plant transpiration. While many studies have investigated the effects of climate change on actual *E*, the complex interactions between the atmosphere, land surface, soil moisture, and vegetation make it challenging to accurately predict changes in *E*. There are few long-term observational records of *E*, forcing a reliance on indirect methods to determine *E* trends at global and decadal scales. Our understanding of changes in *E* remains limited, exemplified by a substantial uncertainty in its estimated long-term changes (Pan et al., 2020; Yang et al., 2023) and a prolonged scientific debate about the impact of warmer and drier atmospheric conditions on future changes in *E* (Ault, 2020; McColl, Roderick, Berg, & Scheff, 2022; Milly & Dunne, 2016; Scheff, Coats, & Laguë, 2022; Sherwood & Fu, 2014; Sergio M. Vicente-Serrano, McVicar, Miralles, Yang, & Tomas-Burguera, 2020; Wang et al., 2022; Zaitchik, Rodell, Biasutti, & Seneviratne, 2023).

The complexity of discerning the influence of anthropogenic climate change on *E* is further complicated by the reciprocal relationship between *E* and the atmospheric state. Atmospheric conditions not only serve as drivers of *E* but also are influenced by *E*, given that *E* acts as a significant moisture source to the air, particularly in inland regions (Gentine, Chhang, Rigden, & Salvucci, 2016; Kim, Garcia, Black, & Johnson, 2023; Kim et al., 2021; McColl, Salvucci, & Gentine, 2019; McColl & Tang, 2024; Vargas Zeppetello et al., 2023). Consequently, the uncertainty in *E* predictions has been identified as a significant contributor to uncertainty in atmospheric state predictions (Dong, Lei, & Crow, 2022; H.-Y. Ma et al., 2018). Paradoxically, however, the impacts of *E* on the near-surface atmosphere are frequently overlooked under the prevailing assumption that the atmospheric state acts primarily as a demand-side driver of *E* (Sergio M. Vicente-Serrano et al., 2020).

Near-surface atmospheric observations in recent decades demonstrate an emergent decline in relative humidity (*RH*) over land (Simmons, Willett, Jones, Thorne, & Dee, 2010; Willett et al., 2014). This decline in observed *RH* over land is commonly explained using an ocean-influence theory (Byrne & O’Gorman, 2016, 2018; Chadwick, Good, & Willett, 2016). This theory suggests that the amplified land warming compared to ocean warming is the primary cause of the *RH* decline since moisture advection from the ocean to the land is insufficient to maintain *RH* over land relative to increasing land surface temperatures. Consequently, warmer and drier atmospheric conditions over land are widely considered to drive a rapid increase in the atmospheric evaporative demand that could intensify *E* (Sherwood & Fu, 2014). However, this perspective ignores the reciprocal influences of *E* and the atmospheric state (Berg & Sheffield, 2018; Kim, Garcia, & Johnson, 2023; S. M. Vicente-Serrano et al., 2018). For example, recent studies suggest that soil moisture constrains moisture supplied to the air through *E*, and this *E*-influenced process is crucial to represent changes in *RH* over land in climate simulations (Berg et al., 2016; Zhou, Leung, & Lu, 2023).

Therefore, it is essential to theoretically harmonize the influences on the atmospheric moisture budget over land resulting from (i) terrestrial *E* and (ii) advected moisture from the ocean. This is particularly important as state-of-the-art climate models currently underestimate the well-established *RH* decline trend (H. Douville & Plazzotta, 2017; Dunn, Willett, Ciavarella, & Stott, 2017; Simpson et al., 2024). However, the fundamental reason for this bias remains unclear (Allan et al., 2020). More importantly, this *RH* bias in climate models implies an underestimation of future drying and warming trends in model projections (Hervé Douville & Willett, 2023). Therefore, a nuanced understanding of the influences of *E* on near-surface humidity trends over land is essential for accurately projecting future atmospheric conditions, water availability, and impacts of anthropogenic climate change on future droughts and wildfires.

Here, we aim to harmonize the influence of terrestrial *E* with the ocean-influence theory to more completely represent *RH* over land within an analytical framework. To this end, we first introduce a simple analytical equation explaining the relationship between changes in specific humidity and *E* from a parsimonious boundary layer moisture budget, and evaluate the proposed equation using in-situ *E* observations from the FLUXNET2015 dataset (Pastorello et al., 2020). We then integrate this equation representing the emerging *E*-influence theory with the ocean-influence theory. Using the ERA5 (Hersbach et al., 2020) and JRA-3Q (Kosaka et al., 2024) reanalysis datasets and 27 general circulation models (GCMs) contained in the Coupled Model Intercomparison Project Phase 6 (CMIP6) (Eyring et al., 2016), we evaluate this integrated framework. In this way, we are able to analyze the physical constraints of changes in *E* and explain why CMIP6 climate models underestimate the emergent *RH* decline present in observations and reanalysis datasets.

Results

E-influence theory

We begin by empirically assessing divergent theories regarding water vapor sources over land. On the one hand, it has been widely hypothesized that horizontal advection from the ocean is the primary source of water vapor over land (Sherwood & Fu, 2014), forming the theoretical foundation of the ocean-influence theory (Byrne & O'Gorman, 2016; Chadwick et al., 2016). However, other studies emphasize a dominant role for *E* as a moisture source to the air, especially for inland regions (Chen, McColl, Berg, & Huang, 2021; McColl & Rigden, 2020; McColl et al., 2019).

We explore these conflicting hypotheses by examining the spatial variability of specific humidity (q, kg kg^{-1}) as a function of distance from the ocean (Fig. 1). On average, the ratio of specific humidity over land (q_L) to specific humidity over the ocean (q_O) decreases rapidly from the coast to ~250 km inland, stabilizing thereafter for areas further inland. This finding that q_L is closer to q_O for areas closer to the coast suggests that horizontal advection from the ocean may be a significant source of water vapor for areas located up to 250 km inland (constituting approximately 40% of the total land area, Fig. 1). However, horizontal advection of q_O appears to become relatively negligible for areas located further inland (i.e., > 250 km), where small horizontal gradients in q_L/q_O suggest that specific humidity in inland regions could be more significantly influenced by *E*. In fact, we find that q_L/q_O is nearly constant (i.e., $\frac{d}{dx}(\frac{q_L}{q_O}) \approx 0$) for areas located between 250 km and 1000 km from a coast, which represents another 40% of the total land area. Further declines in q_L/q_O for areas >1000 km inland imply increasing moisture limitations typical of arid regions.

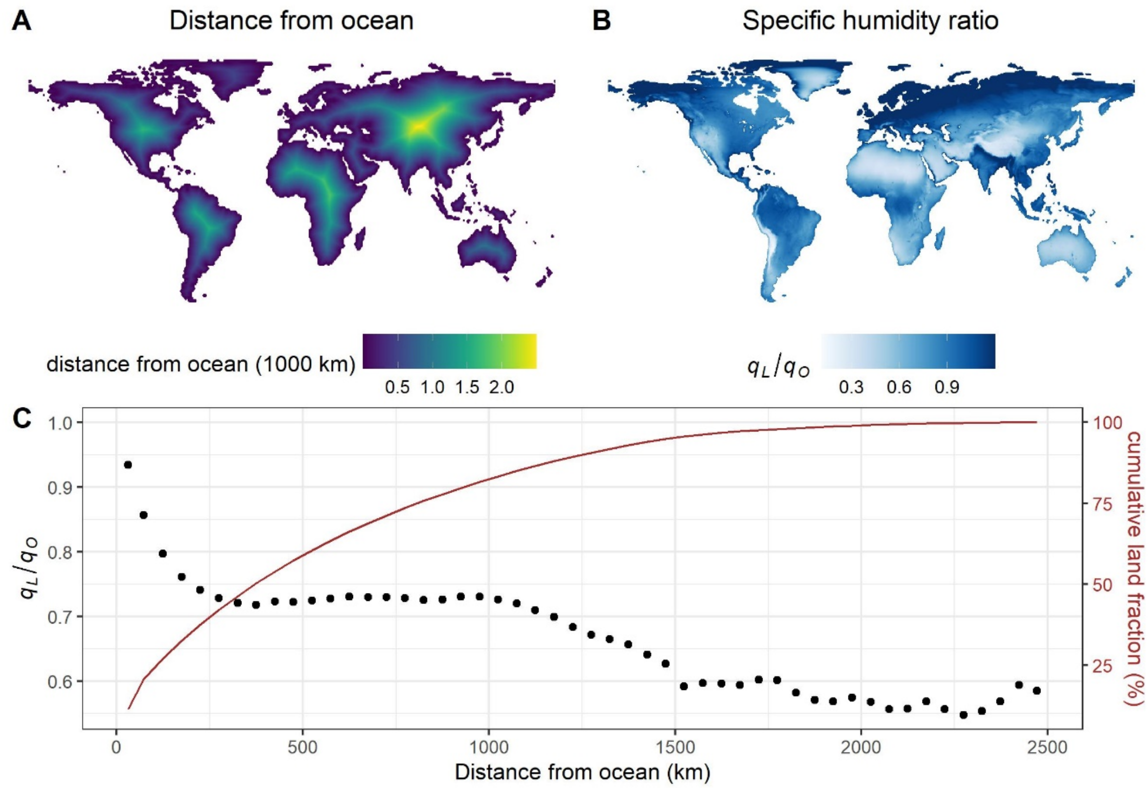

Fig. 1. Mean specific humidity ratio between land and ocean plotted against the distance from ocean. (**A**) Global map indicating the distance from ocean. (**B**) Global map of the mean specific humidity ratio between land (q_L) and ocean (q_O) in the ERA5 reanalysis over the period 1973-2022. The time-averaged q_L is calculated for each grid, while the time-averaged q_O is determined as the zonal mean at that latitude to represent the neighboring ocean. (**C**) Relationship between q_L/q_O and the distance from ocean. The black dot represents the mean q_L/q_O, calculated for binned distances from the ocean (each bin has 50 km). The cumulative land fraction (brown line) is included as a reference.

The empirical, emergent characteristics of $\frac{d}{dx}(\frac{q_L}{q_O})$ in Fig. 1 prompts a reexamination of the derivation of the ocean-influence theory, given that horizontal advection (driven by horizontal q gradients) doesn't always emerge as the predominant moisture source, particularly over inland regions. Byrne and O'Gorman (2016) proposed a parsimonious steady-state moisture budget for a boundary layer box over land (Fig. S1), which assumes negligible E in order to derive a simple moisture constraint, as expressed by Eq. 1:

$$\Delta q_L = \frac{q_L}{q_O}\Delta q_O \qquad (1)$$

where Δ indicates the temporal change between two periods. Eq. 1 is a summary of the ocean-influence theory, which was introduced to explain the observed decline in *RH* over land using ocean advection (Byrne & O'Gorman, 2016, 2018; Chadwick et al., 2016). The derivation of Eq. 1 involved assumptions of constant values for horizontal and vertical mixing velocities, boundary layer heights, and the specific humidity jump rate at the top of the boundary layer.

To maintain compatibility with this theoretical framework, we adopt the same moisture budget equation and assumptions for Eq. 1 while considering horizontal advection as negligible, focusing instead on the influence of *E*. In this scenario, the changes in specific humidity over land can be expressed as follows (for detailed derivation, refer to Materials and Methods):

$$\Delta q_L = \frac{q_L}{E}\Delta E \tag{2}$$

Eq. 2 is the proposed theoretical constraint for changes in q_L and E when horizontal moisture advection is negligible and thus q_L is predominantly controlled by *E*. By rearranging Eq. 2 for ΔE and partitioning Δq_L into *RH* and temperature components, we can write as follows.

$$\Delta E = \frac{E}{q_L}\Delta q_L$$

$$= \frac{E}{RH_L}\Delta RH_L + \alpha E \Delta T_L \tag{3}$$

where $RH_L(=\frac{q_L}{q^*(T_L)})$ is the near-surface *RH* over land, $q^*(T_L)$ is saturation specific humidity at the near-surface air temperature (T_L), $\alpha(=\frac{s}{q^*(T)})$ is the sensitivity of saturation specific humidity to temperature, and $s(=\frac{dq^*}{dT})$ is the linearized saturation specific humidity slope versus temperature. Here, we approximate *RH* using specific humidity instead of water vapor pressure and linearize the Clausius-Clapeyron relationship.

Eq. 3 implies that one can simply determine ΔE only using atmospheric observations. However, while Eq. 1 has undergone evaluation in several prior studies (Byrne & O'Gorman, 2016, 2018; Chadwick et al., 2016; Seltzer, Blard, Sherwood, & Kageyama, 2023), the viability of the proposed Eq. 3 demands a comprehensive assessment. Evaluating the proposed theory represented by Eq. 3 presents a challenge due to the absence of reliable long-term ΔE observations, particularly at global scale, given that *E* is more challenging to observe than specific humidity.

Alternatively, we assessed the feasibility of Eq. 3 using observed seasonal changes in ΔE at the field scale (e.g., a few square kilometers). We used FLUXNET2015 monthly-scale *E* and meteorological observations from 170 sites worldwide (Pastorello et al., 2020). We estimated ΔE from Eq. 3 using monthly differences in RH_L and T_L. Subsequently, we compared observed values for ΔE with those estimated for ΔE using Eq. 3. We find that Eq. 3 effectively estimates the observed ΔE, particularly in inland regions (Fig. 2). The majority of inland sites (> 250 km from the ocean) exhibit a high correlation coefficient (*R*) between observed ΔE and its estimation using Eq. 3, with regression slopes close to one. On the other hand, the correlation between ΔE and its estimation form Eq. 3 is lower for several sites located closer to a coast (<= 250 km from ocean). These field-scale results support the viability of the proposed Eq. 3, especially in inland regions where horizontal moisture advection from the ocean becomes increasingly negligible for increasing distance from the coast. It is worth noting that the robustness of this result persisted when substituting the *E* observations with the energy balance-corrected version of *E* (see Fig. S2).

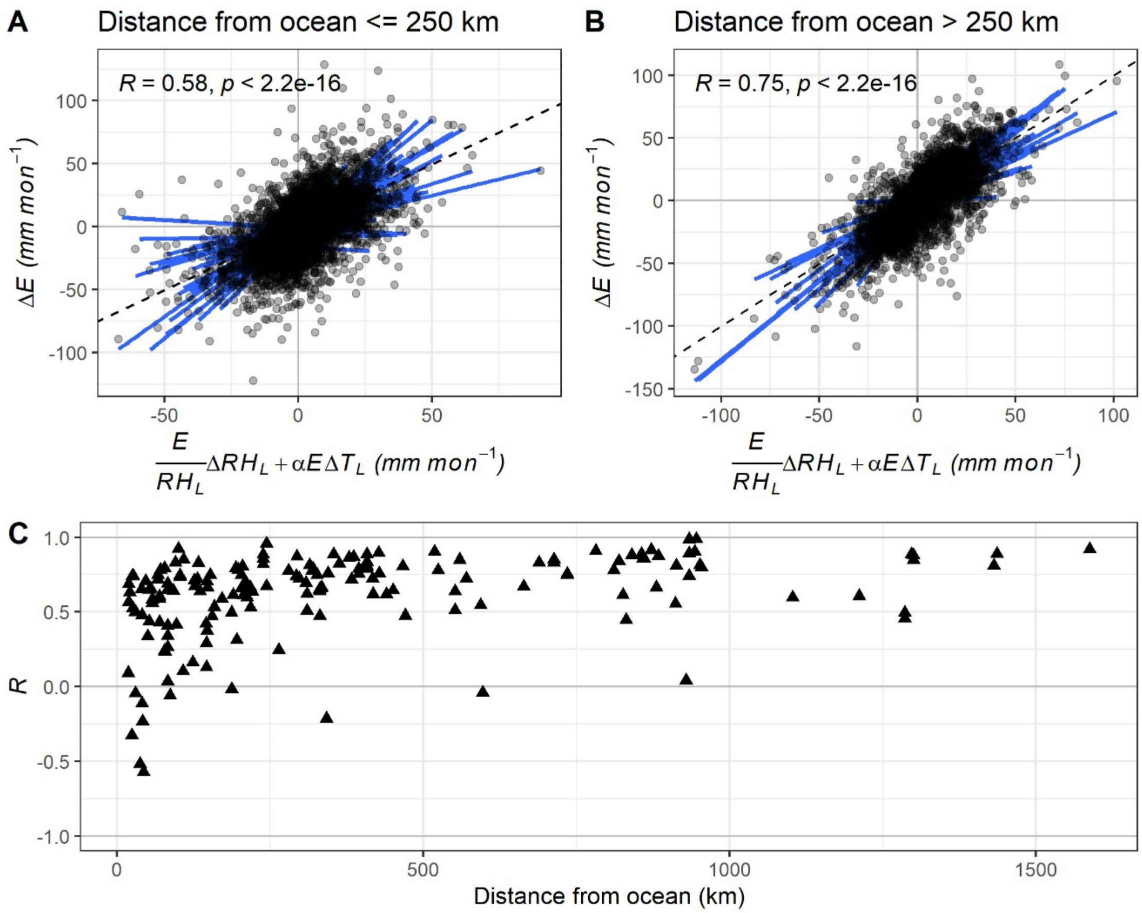

Fig. 2. Evaluation of Eq. 3 at regional scale using FLUXNET2015 dataset. Scatter plot depicting ΔE and its estimation using Eq. 3 for (**A**) pericoastal sites (distance from the ocean ≤ 250 km) and (**B**) inland sites (distance from the ocean > 250 km). Blue lines represent linear regression lines for each site, and black dashed lines indicate one-on-one lines. (**C**) Correlation (R) between ΔE and $\frac{E}{RH_L}\Delta RH_L + \alpha E \Delta T_L$ for each site (y-axis) versus the distance from the ocean for each site (x-axis).

While the evaluation at field and seasonal scales supports Eq. 3, it is important to note that the direct applicability of Eq. 3 for inferring long-term changes in global land E remains to be established. We also note that the omission of horizontal advection from the ocean in the derivation of Eq. 3 is unrealistic on a global scale, necessitating an additional line of inquiry. To further assess the performance of Eq. 3 at the global level, we employed modeled ΔE and atmospheric state from two latest generation reanalysis datasets and from climate simulations, assuming that ΔE and atmospheric state in each climate model represent internally consistent representations of the land-atmosphere-ocean coupled system (Milly & Dunne, 2016). Specifically, we focus on non-Polar regions located 66.5°S to 66.5°N in order to exclude the Artic and Antarctica since the ocean-influence theory is better justified at lower latitudes (Byrne & O'Gorman, 2018).

Our analysis revealed that Eq. 3 consistently overestimates global land ΔE for the recent 43 years (1980-2022) in ERA5 and JRA-3Q reanalysis datasets (Fig. 3), as well as for all 27 GCMs in CMIP6 (Fig. 4). This suggests a systematic bias in Eq. 3 on the global scale, despite its reasonable performance at the regional level. At the regional scale, horizontal moisture advection can be both positive and negative, depending on the dryness of nearby regions, but horizontal advection from ocean to land is always positive at the global scale as q_O is always greater than q_L. Therefore, Δq_L not only increases due to the rise in E, but also increases due to heightened ocean advection that is driven by the increasing q_O in a warming climate. Consequently, the simplifying assumptions of Eq. 3 lead to overestimation of global-scale changes in E, suggesting that an additional term is needed to represent the influence of ocean advection. We now turn our attention to incorporating ocean advection into Eq. 3.

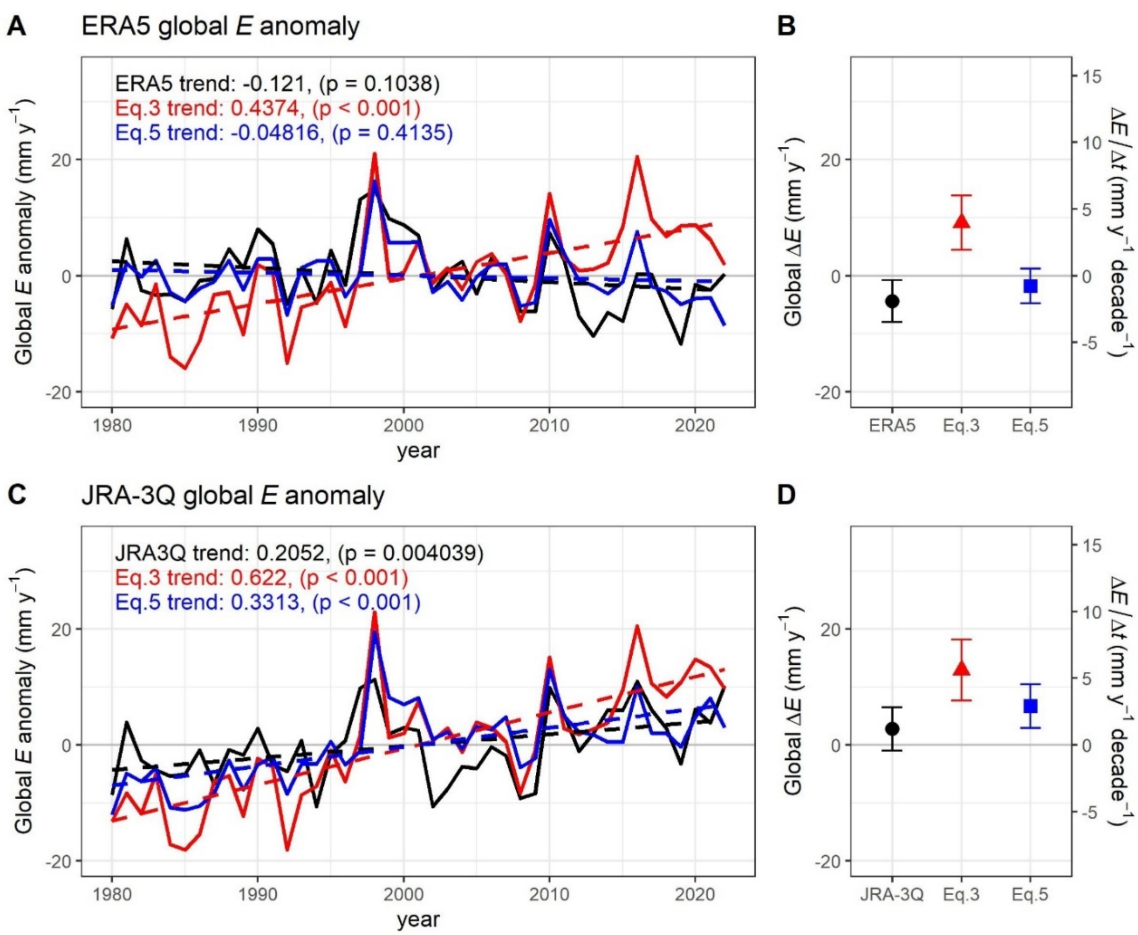

Fig. 3. Evaluation of Eq. 3 and Eq. 5 at global scale relative to ERA5 and JRA-3Q reanalysis datasets. (**A**) Global land E anomaly from ERA5 reanalysis (black), Eq. 3 (red), and Eq. 5 (blue) over the period 1980-2022. Dashed lines represent linear trends. (**B**) Global ΔE from ERA5 reanalysis (black), Eq. 3 (red), and Eq. 5 (blue), calculated as the difference between current (2003-2022) and past climate (1980-1999). Error bars represent the 95% confidence intervals, and the secondary y-axis shows the average rate of change. (**C**) Similar to panel (A) but using JRA-3Q reanalysis. (**D**) Similar to panel (B) but using JRA-3Q reanalysis. In this figure, Eqs. 3 and 5 are calculated using atmospheric variable from each reanalysis, and the artic (>66.5°N) and antarctica (<66.5°S) are masked.

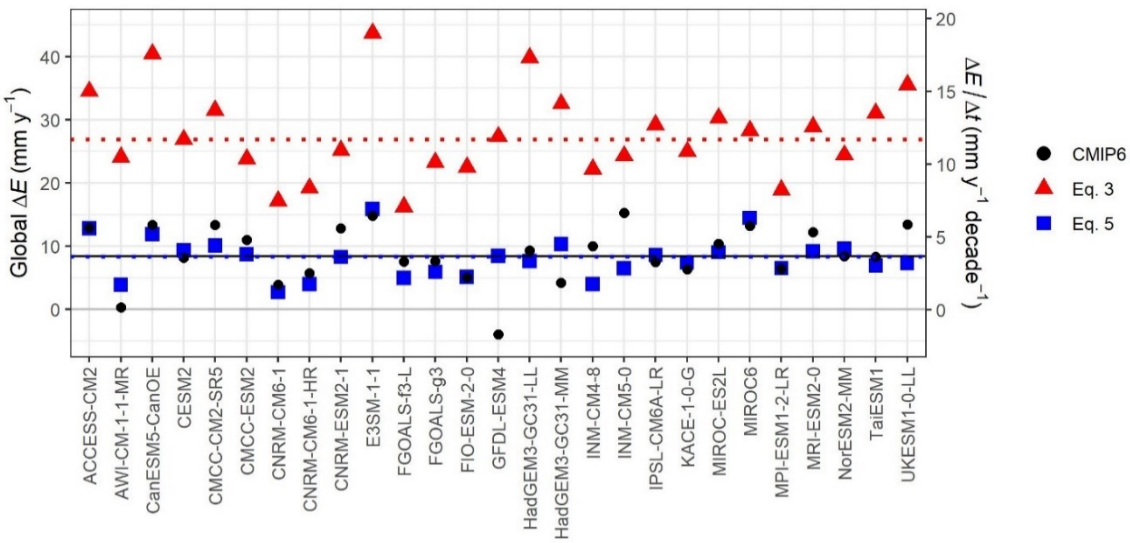

Fig. 4. Evaluation of Eq. 3 and Eq. 5 at global scale using CMIP6 climate models. Global ΔE from each climate model (black), Eq. 3 (red), and Eq. 5 (blue), calculated as the difference between current (2003-2022) and past climate (1980-1999). Dotted lines indicate median of Eq. 3 (red) and Eq. 5 (blue) while the black solid line indicates median of CMIP6. In this figure, Eqs. 3 and 5 are calculated using atmospheric variables, and polar regions (>66.5°N and <66.5°S) are masked.

Reintroducing ocean advection

While the findings using Eq. 3 shows promise in providing a simple constraint on ΔE based solely on meteorological observations for land, it is essential to account for horizontal advection from the ocean to adequately constrain the long-term trend of E on a global scale. In the Materials and Methods, we merge the ocean-influence theory and the proposed E-influence theory as follows:

$$\Delta E = \frac{E}{q_L}\left(\Delta q_L - \frac{q_L}{q_O}\Delta q_O\right) \quad (4)$$

Eq. 4 considers both E and ocean advection in constraining Δq_L, thus providing a more comprehensive framework for understanding the dynamics of moisture transfer. Here, the second term of the right-hand side represents horizontal ocean advection. An intriguing aspect is that if the ocean-influence theory summarized by Eq. 1 is true, the right-hand side of Eq. 4 becomes zero, implying no increase in E.

In order to explicitly consider relationships between RH_L, temperature, and E, we decompose Δq into RH and temperature components similar to Eq. 3. Here, we assume time constant RH over ocean (Held & Soden, 2006; O'Gorman & Muller, 2010), resulting in the following expression:

$$\Delta E = \frac{E}{RH_L}\Delta RH_L + \alpha E(\Delta T_L - \Delta T_O) \quad (5)$$

where T_O is near-surface temperature over the ocean. The ocean advection term in Eq. 4 is embedded in the last term of the right-hand side of Eq. 5.

Equation 5 serves as our proposed model to estimate the long-term trend of E on a global scale using atmospheric variables and accounting for ocean advection. Consistent with the previous section, we apply Eq. 5 to ERA5 and JRA-3Q reanalysis data and CMIP6 GCMs due to the absence of long-term global land ΔE observations.

Our results show that Eq. 5 effectively reproduces the direct ΔE output from reanalysis (Fig. 3). Furthermore, not only does it capture the long-term ΔE, but Eq. 5 also reasonably replicates the interannual variability of global land E particularly in the ERA5 climate reanalysis dataset (R=0.69). Also, ΔE estimations using Eq. 5 exhibit a much closer match with the direct ΔE output from CMIP6 GCMs compared to Eq. 3.

Discussion

Reconciling with the ocean-influence theory

Byrne and O'Gorman (2018) demonstrated that a simple ocean advection constraint, as summarized in Eq. 1, along with another constraint on moist static enthalpy, can explain the observed decline in RH over land. At first glance, this ocean-influence theory may seem to be in contradiction with our proposed theoretical framework. However, reconciliation between the two theoretical frameworks is possible if ΔE is close to zero in Eq. 4, as illustrated in the previous section.

Indeed, our analysis reveals that there are no significant global land E trends in ERA5 and JRA-3Q reanalysis for the past 43 years, although ERA5 suggests a slightly negative trend and JRA-3Q suggests a slightly positive trend. These subtle global land E trends are effectively replicated by our theoretical model of Eq. 5 (Fig. 3). These results suggest that the conventional ocean-influence theory and the present work can both be compatible within ERA5 and JRA-3Q reanalysis, which is known to assimilate in situ humidity observations and thus accurately reproduce the observed declining trend of RH_L (Dunn et al., 2017; Simpson et al., 2024).

On the other hand, most CMIP6 GCMs estimate positive global land E trends for the past 43 years (Fig. 4). This suggests that the left-hand side of Eq. 4 is positive, implying $\Delta q_L > \frac{q_L}{q_O}\Delta q_O$ and contradicting the ocean-influence theory summarized in Eq. 1. In other words, if an increase in q_L is faster than the rate suggested by the ocean-influence theory, it could imply an intensification of global land E. Recently, Seltzer et al. (2023) found that the paleotemperature proxies suggested $\Delta q_L = 0.84\Delta q_O$, where 0.84 is approximately 10-20% larger than recent observations of $\frac{q_L}{q_O}(= 0.72)$ at the global scale (Byrne & O'Gorman, 2018). This implies that changes in q_L are faster than the rate suggested by the ocean-influence theory at the last glacial maximum, and it could potentially signify changes in E within the context of Eq. 4. Consequently, our theoretical framework remains consistent with recent paleotemperature proxies as well.

Why do CMIP6 models underestimate the observed decline in *RH* over land?

To gain a deeper insight into the drivers behind RH_L decline in recent decades, we reorganize the proposed theory (Eq. 5) and the ocean-influence theory (Eq. 1) as follows:

$$\Delta RH_L = \overbrace{\underbrace{\frac{RH_L}{E}\Delta E}_{from\,E} + \underbrace{\alpha RH_L \Delta T_O}_{from\,ocean}}^{water\ vapor\ supply} - \overbrace{\alpha RH_L \Delta T_L}^{warming} \quad (6)$$

$$\Delta RH_L = \overbrace{\alpha RH_L \Delta T_O}^{\substack{water\ vapor\ supply \\ from\ ocean}} - \overbrace{\alpha RH_L \Delta T_L}^{warming} \tag{7}$$

Eq. 6 describes changes in RH_L according to the proposed theory, while Eq. 7 describes changes in RH_L according to the ocean-influence theory. The sole disparity between the two equations lies in the initial term of Eq. 6, which represents the water vapor supply from E. RH_L can decline if the increase in water vapor supply is slower than the increase in saturation vapour pressure resulting from atmospheric warming. On the other hand, RH_L may remain steady if the water vapor supply is sufficiently large to offset the warming effect of increasing atmospheric moisture storage capacity due to the Clausius-Clapeyron relation. Therefore, decomposing ΔRH_L into three components using Eq. 6 can help identify the primary sources of the difference between reanalysis and CMIP6 climate models.

Fig. 5 presents the results of applying Eqs. 6 and 7 to the two reanalysis datasets and CMIP6 GCMs. The first column shows that the decline in RH_L is underestimated in CMIP6 models compared to ERA5 and JRA-3Q. The second column demonstrates that Eq. 6 can reasonably replicate this difference in terms of the ensemble median ΔRH_L, although CMIP6 models exhibit more variability. If we omit the first term of Eq. 6 as implied in Eq. 7, ΔRH_L from CMIP6 aligns closely with reanalysis (third column of Fig. 5). This result implies that the difference in ΔE between CMIP6 and reanalysis is a significant contributor to the ΔRH_L bias.

Specifically, we found that the difference in water vapor supply from E between reanalysis and CMIP6 is sufficient to account for the difference in ΔRH_L between the two. The ocean advection term is also higher in CMIP6 than in reanalysis, but this effect roughly cancels out as terrestrial warming is also higher in CMIP6 than in reanalysis. This implies that the larger ocean warming in CMIP6 compared to observations in the recent decade cannot entirely explain the ΔRH_L bias in CMIP6 because the amplified terrestrial warming is also higher in CMIP6. This result aligns with recent studies (Hervé Douville et al., 2020; Simpson et al., 2024), which demonstrated that climate models prescribing observed ocean warming cannot completely resolve the ΔRH_L bias issue.

Our analysis implies a potential overestimation of the intensification of terrestrial E in climate simulations, leading to a bias in ΔRH_L. This interpretation aligns with findings from a recent study (Hervé Douville & Willett, 2023), which identified certain plausible climate models within CMIP6 that exhibit a drier ΔRH_L. Notably, these plausible models generally demonstrate a weaker increase in terrestrial E compared to other models, supporting our interpretation. If the intensification of terrestrial E is indeed exaggerated in current state-of-the-art climate models, and if future projections also suffer from the same issue, as indicated by Hervé Douville and Willett (2023), several significant implications may arise.

Firstly, the anticipated reduction in future soil moisture could be more severe than currently predicted by most models included in CMIP6. This is consequential because soil moisture reduction serves as a primary driver of the limited increase in terrestrial evapotranspiration, leading to a decline in RH in climate models (Berg et al., 2016; Zhou et al., 2023). Secondly, the future ratio between annual mean runoff and annual mean precipitation (i.e., runoff ratio) might be underestimated due to the overestimated terrestrial evapotranspiration (Hervé Douville & Willett, 2023). The underestimated runoff ratio could imply a miscalculation of extreme flood events in the future based on current climate model projections. Thirdly, in alignment with the concerns raised by a recent study (Simpson et al., 2024), the danger of wildfires and heatwaves may be more severe than predicted based on current climate models. If future terrestrial evapotranspiration is constrained ($\Delta E \approx 0$), while *RH* decreases and temperature increases, extremely dry and hot weather conditions could become even more severe (Byrne, 2021). These implications highlight the importance of accurately modeling terrestrial evapotranspiration for a comprehensive understanding of future climate-related risks.

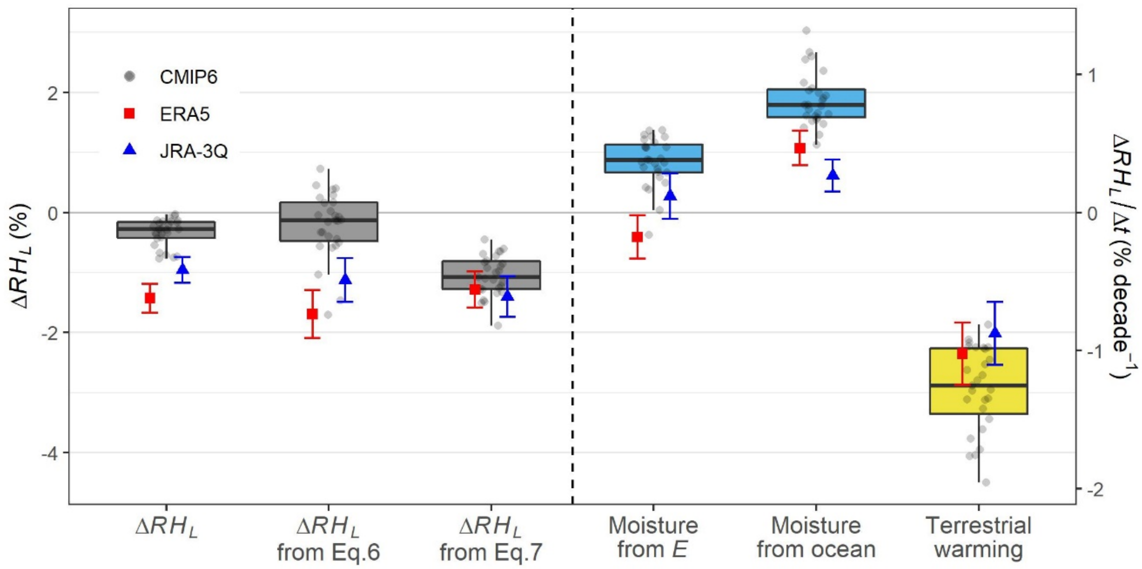

Fig. 5. Attribution of ΔRH_L based on Eq. 6. Box plots with jitter points depict CMIP6 models, while the red squares with error bars represent ERA5, and the blue triangles with error bars represent JRA-3Q. The first column is ΔRH_L, the second column is the estimated ΔRH_L using Eq. 6, and the third column is the estimated ΔRH_L using Eq. 7. The last three columns provide a breakdown of each term in Eq. 6. Here Δ indicates difference between current (2003-2022) and past climate (1980-1999). Error bars represent the 95% confidence intervals, and the secondary y-axis shows the average rate of change.

Theoretical upper limit of increases in global *E*

Although our initial, simplified *E*-influence theory in Eq. 3, which ignores ocean advection, tends to overestimate the global trend of *E* (Figs. 3 and 4), it provides a clear upper limit for the increase in global *E* based on the observed humidity trend over land. Specifically, considering that the ERA5 and JRA-3Q reanalysis closely aligns with the current trend of *RH* observations compared to climate simulations, Eq. 3 calculated using reanalysis meteorological data in Fig. 3 (i.e., 4 ~ 6 mm y^{-1} $decade^{-1}$) could serve as an upper limit for the increase in global *E* over past decades. It is unlikely for the global *E* increase to surpass this limit unless specific humidity over the ocean decreases, a scenario deemed unrealistic under a warming climate (Allan, Willett, John, & Trent, 2022; Xu et al., 2024).

This upper limit based on humidity observations holds significance due to the substantial uncertainty in estimating the long-term global trend of *E* (Pan et al., 2020; Yang et al., 2023). While recent water balance *E* estimations suggest a slight decreasing *E* trend (N.

Ma, Zhang, & Szilagyi, 2024), numerous remote sensing-based E estimates, employing physical equations or empirical models, exceed 4 ~ 6 mm y^{-1} $decade^{-1}$ (Pan et al., 2020; Yang et al., 2023). Physically based E estimates from remote sensing often heavily depend on increases in temperature and net radiation, with the decrease in RH_L rarely considered or treated as an increase in E based on the atmospheric evaporative demand concept. However, our theory and analysis consistently demonstrate that a decrease in RH_L over this decadal time scale should not be interpreted as an increase in E. Rather, the decrease in RH_L should be understood as a consequence of a smaller increase in E to the water vapour supply within a coupled atmospheric boundary layer. This discrepancy in perspective may contribute to biases in physically based E estimations.

As for empirical models (e.g., machine learning models), a common approach involves upscaling empirical relationships between meteorological variables, remote sensing data, and E. Since Eq. 3 effectively constrains regional-scale ΔE, any bias in short-term and regional-scale training could potentially manifest when scaled up to longer time scales and global spatial scales. Our findings, indicating that Eq. 3 works well at a regional scale (Fig. 2) but introduces systematic bias at a global scale (Figs. 3 and 4), underscore the importance of recognizing that the relationship between E and atmospheric variables can vary depending on the scale. Due to their lack of constraint by physical principles such as ocean advection, empirical models may inherently include systematic biases.

Potential caveats and outlook.

In this study, we present simple theoretical frameworks based on meteorological information to elucidate the source variability in E for climate models vs. observational data and reanalysis products. We employed this approach to evaluate trends in atmospheric humidity and E over past decades, particularly on a global scale. While our theory aligns consistently with observations, reanalysis, and climate models, certain limitations should be acknowledged in our methodology.

Firstly, our simple physical model relies on several simplified assumptions. For instance, Eq. 3 neglects local horizontal moisture advection, which could be a significant factor. Although Eq. 5 is introduced to account for horizontal moisture advection, it is only plausible at a global spatial scale, and therefore, it cannot accurately represent horizontal moisture advection at local scale. Consequently, our approach is not suitable for assessing regional scale long-term changes in E. A future study could enhance the model's regional scale applicability by incorporating additional advection terms into Eq. 5 or 3, providing a more accurate representation of local advection processes to understand regional changes in E.

Secondly, our approach is an analytical model instead of a process-based model, and as such, it cannot explain why E remained steady in reanalysis and was overestimated in CMIP6 climate simulations. This discrepancy could be related to surface parameterizations, considering factors such as stomatal closure due to the CO_2 fertilization effect (Hervé Douville et al., 2020). Soil moisture limitation on E is another potential mechanism (Berg et al., 2016; Zhou et al., 2023). To better grasp the origin of this issue, future studies may explore the relationship between satellite soil moisture, E, and atmospheric humidity. Also, it is important to conduct experiments using land surface models with varying parameters or model structures to better understand the origin of the bias.

Materials and Methods

FLUXNET2015 data

To assess the proposed Eq. 3, we used the FLUXNET2015 Tier One (CC-BY-4.0) dataset (Pastorello et al., 2020). This global dataset includes 212 in-situ eddy-covariance flux tower sites around globe representing over 1,500 site years. Monthly records of latent heat flux, air temperature, vapor pressure deficit, and air pressure were obtained from the FLUXNET data portal (https://fluxnet.org/data/fluxnet2015-dataset/). We only included data for periods for which the quality control flag indicated more than 80% of the half-hourly data were used for generating the monthly datasets (i.e., measured data or good quality gap-filled data). Also, we only included data points with positive latent heat flux. Additionally, we considered only sites with at least three consecutive months of available data. Following these filtering processes, 170 flux sites around the globe were retained.

The calculation of E was derived from latent heat flux, α from temperature, and RH from temperature, air pressure, and vapor pressure deficit using the bigleaf R package (Knauer, El-Madany, Zaehle, & Migliavacca, 2018). The multiplications of ΔRH_L and ΔT_L in Eq. 3 were averaged values over the two months, with ΔRH_L and ΔT_L calculated as the difference between the two months. In Fig. 2, observed latent heat flux, without energy balance correction, was employed. Notably, we found similar results when using the energy balance correction version of latent heat flux, incorporating the Bowen ratio preservation method (Pastorello et al., 2020; Twine et al., 2000) (see Fig. S2).

ERA5 and JRA-3Q reanalysis

To evaluate the proposed theoretical framework, we employed ERA5, the latest reanalysis product from the European Center for Medium Range Weather Forecasts (ECMWF) (Hersbach et al., 2020), and JRA-3Q, the latest reanalysis product from the Japan Meteorological Agency (Kosaka et al., 2024). It is worth noting that, in this study, we deliberately excluded MERRA2 reanalysis, another widely used reanalysis product by the National Aeronautics and Space Administration (NASA). This decision was based on MERRA2's limitation of not assimilating in situ humidity observations and its documented tendency to overestimate specific humidity trends (Simpson et al., 2024).

We obtained ERA5 single level (near-surface) output from the Climate Data Store (CDS) of ECMWF (https://doi.org/10.24381/cds.f17050d7), and JRA-3Q single level (near-surface: 2 m height) output at 1.25 degree spatial resolution from the Data Integration and Analysis System (DIAS) (https://doi.org/10.20783/DIAS.645). We obtained monthly records of latent heat flux, air pressure, air temperature, and dewpoint temperature for the period of 1980-2022. We then calculated E from latent heat flux, α from temperature, and RH from temperature, air pressure, and dewpoint temperature using the bigleaf R package (Knauer et al., 2018).

CMIP6 models

In addition to the two reanalysis datasets, we incorporated data from 27 climate models within the CMIP6 (Eyring et al., 2016). The complete list of the utilized climate models is detailed in Table S1. For the analysis, we employed the Historical simulation covering the period from 1980 to 2014. Given that the historical simulation ended in 2014, we augmented our dataset with Shared Socioeconomic Pathway 5-8.5 (SSP5-8.5) simulations for the subsequent period from 2015 to 2022 to ensure comparability with the reanalysis datasets. We obtained monthly scale climate models' output from CDS of ECMWF (https://doi.org/10.24381/cds.c866074c). Latent heat flux, near-surface air temperature, near-surface air specific humidity, and surface air pressure were retrieved. We then calculated E from latent heat flux, α from temperature, and RH from temperature, air pressure, and specific humidity.

Derivation of the *E*-influence theory

Byrne and O'Gorman (2016) introduced an idealized atmospheric boundary layer (ABL) box model to elucidate the relationship among horizontal moisture advection from the ocean, terrestrial E, and the vertical relaxation flux of moisture at the top of the ABL (e.g., entrainment). This idealized box model assumes a fixed ABL height and can be conceptualized as a diel-averaged ABL, similar to another ABL box model introduced elsewhere (McColl et al., 2019; Vargas Zeppetello et al., 2023). The moisture budget within the ABL box over land can be expressed as follows (Fig. S1):

$$h_L \frac{dq_L}{dt} = \frac{h_O}{l} \rho v_1 (q_O - q_L) + \frac{h_L - h_O}{l} \rho v_1 \left(q_{FT,O} - q_L\right) + \rho v_2 \left(q_{FT,L} - q_L\right) + E \qquad (8)$$

where h is the boundary layer height, l is the length of the land, q is specific humidity, v_1 is horizontal mixing velocity, v_2 is vertical mixing velocity, and ρ is the air density. The subscripts O and L respectively denote ocean and land, while the subscript FT indicates the free troposphere immediately above the land and ocean boundary layers. Under steady-state conditions, the right-hand side is set to zero (i.e., $\frac{dq_L}{dt} = 0$). Byrne and O'Gorman (2016) further simplified Eq. 8 by assuming that the free-tropospheric specific humidity is directly proportional to the ABL specific humidity, denoted as $q_{FT,L} = \lambda_L q_L$ and $q_{FT,O} = \lambda_O q_O$, where λ_L and λ_O are time constants. This assumption is also consistent with another derivation of the ocean-influence theory based on Lagrangian path-integral (Chadwick et al., 2016), where they assumed λ_L to be zero.

While the prior study focused on the horizontal advection from the ocean by assuming negligible E, we assume negligible horizontal advection. This assumption is justifiable in inland regions where horizontal specific humidity differences are minimal (see Fig. 1). Mathematically, the assumption of negligible horizontal advection can be expressed by considering $l \to \infty$ in Eq. 8, resulting in the following expression:

$$q_L = \frac{1}{\rho v_2 (1 - \lambda_L)} E \qquad (9)$$

or

$$q_L = \beta E \qquad (10)$$

where $\beta = 1/\rho v_2 (1 - \lambda_L)$, which depends primarily on the vertical mixing velocity at the top of the ABL. At a climatically-relevant time scale and a global spatial scale, β could be considered time constant because (1) changes in v_2 can be damped by multiplication by $1 - \lambda_L$, and (2) consistent changes in v_2 across all land grid are unrealistic, although significant local-scale changes in v_2 could occur (Chadwick et al., 2016). If we assume β as time constant, β can be understood as a partial derivative of q_L with respect to E. The constant β in Eq. 10 also implies that the ratio of q_L and E remains approximately constant. Therefore, we can write as follows:

$$\frac{\partial q_L}{\partial E} = \beta \quad (11)$$

and

$$\frac{dq_L}{q_L} = \frac{dE}{E} \quad (12)$$

It is worth noting that Eq. 11 is conceptually similar to the sensitivity of the specific humidity to changes in E introduced by McColl et al. (2019). In their work, they also showed that $\frac{\partial q_L}{\partial E}$ is largely governed by the vertical mixing velocity at the top of ABL (i.e., the relaxation conductance in their notation).

Eq. 12 leads to Eq. 2 in the main text.

Merging two theories

In this section, we integrate the E-influence theory and the ocean-influence theory in a simple way. We assume that Δq_L can be linearly partitioned into two components based on their sources:

$$\Delta q_L = \Delta q_E + \Delta q_A \quad (13)$$

where Δq_E represents changes in specific humidity over land attributed to terrestrial E in the absence of ocean advection, while Δq_A represents changes in specific humidity over land due to moisture advection from the ocean in the absence of terrestrial E.

According to the proposed E-influence theory, we can express Δq_E as follows:

$$\Delta q_E = \frac{q_L}{E} \Delta E \quad (14)$$

Similarly, we can express Δq_A based on the ocean-influence theory as follows:

$$\Delta q_A = \frac{q_L}{q_O} \Delta q_O \quad (15)$$

Substituting Eqs. 14 and 15 into Eq. 13 allow us to derive Eq. 4 in the main text.

Application of the proposed equations to reanalysis and GCMs

The proposed Eq. 3 was applied to each land grid cell. Specifically, we first calculated the climatology of the multiplications of ΔRH_L and ΔT_L in Eq. 3 for each month and grid. For the reanalysis applications presented in Fig. 3, the monthly climatology was multiplied by monthly anomalies of RH_L and T_L at each grid cell. The resulting values for each grid cell and month were spatially averaged with cosine-latitude weighting before computing annual average. In the case of CMIP6 climate models depicted in Fig. 4, the monthly climatology was multiplied by ΔRH_L and ΔT_L representing the difference between the current (2003-2022) and past (1980-1999) climate. Similar to the reanalysis dataset, the products were then spatially averaged using cosine-latitude weighting.

The application of Eq. 5 paralleled that of Eq. 3, with the distinction that the ocean temperature term (ΔT_O) needed to be incorporated. ΔT_O was individually computed for each ocean grid cell and subsequently spatially averaged using cosine-latitude weighting to derive the global average. These global averaged ΔT_O values were then introduced to each land grid cell for the application of Eq. 5. The computation of other variables in Eq. 5 followed the same methodology as outlined for Eq. 3.

In generating Fig. 5, which shows the application results of Eqs. 6 and 7, a challenge arose when attempting to apply the equation to each grid cell. This challenge was rooted in the fact that the first term on the right-hand side of Eq. 6 increases infinitely when E approaches zero. To address this issue, $\frac{RH_L}{E}$ was computed as the global mean of RH_L divided by the global mean of E. Subsequently, this global $\frac{RH_L}{E}$ value was multiplied to Eq. 5 to derive Eq. 6, while other variables were calculated at each grid cell and then spatially averaged by following the same methodology as outlined in the above paragraph.

References

Allan, R. P., Barlow, M., Byrne, M. P., Cherchi, A., Douville, H., Fowler, H. J., . . . Zolina, O. (2020). Advances in understanding large-scale responses of the water cycle to climate change. *Annals of the New York Academy of Sciences, 1472*(1), 49-75. doi:10.1111/nyas.14337

Allan, R. P., Willett, K. M., John, V. O., & Trent, T. (2022). Global Changes in Water Vapor 1979–2020. *Journal of Geophysical Research: Atmospheres, 127*(12), e2022JD036728. doi:10.1029/2022JD036728

Ault, T. R. (2020). On the essentials of drought in a changing climate. *Science, 368*(6488), 256-260. doi:10.1126/science.aaz5492

Berg, A., Findell, K., Lintner, B., Giannini, A., Seneviratne, S. I., van den Hurk, B., . . . Milly, P. C. D. (2016). Land–atmosphere feedbacks amplify aridity increase over land under global warming. *Nature Climate Change, 6*(9), 869-874. doi:10.1038/nclimate3029

Berg, A., & Sheffield, J. (2018). Climate change and drought: the soil moisture perspective. *Current Climate Change Reports, 4*(2), 180-191. doi:10.1007/s40641-018-0095-0

Byrne, M. P. (2021). Amplified warming of extreme temperatures over tropical land. *Nature Geoscience, 14*(11), 837-841. doi:10.1038/s41561-021-00828-8

Byrne, M. P., & O'Gorman, P. A. (2016). Understanding decreases in land relative humidity with global warming: conceptual model and GCM simulations. *Journal of Climate, 29*(24), 9045-9061. doi:10.1175/jcli-d-16-0351.1

Byrne, M. P., & O'Gorman, P. A. (2018). Trends in continental temperature and humidity directly linked to ocean warming. *Proceedings of the National Academy of Sciences, 115*(19), 4863-4868. doi:10.1073/pnas.1722312115

Chadwick, R., Good, P., & Willett, K. (2016). A Simple Moisture Advection Model of Specific Humidity Change over Land in Response to SST Warming. *Journal of Climate, 29*(21), 7613-7632. doi:10.1175/JCLI-D-16-0241.1

Chen, S., McColl, K. A., Berg, A., & Huang, Y. (2021). Surface Flux Equilibrium Estimates of Evapotranspiration at Large Spatial Scales. *Journal of Hydrometeorology, 22*(4), 765-779. doi:10.1175/jhm-d-20-0204.1

Dong, J., Lei, F., & Crow, W. T. (2022). Land transpiration-evaporation partitioning errors responsible for modeled summertime warm bias in the central United States. *Nature Communications, 13*(1), 336. doi:10.1038/s41467-021-27938-6

Douville, H., Decharme, B., Delire, C., Colin, J., Joetzjer, E., Roehrig, R., . . . Voldoire, A. (2020). Drivers of the enhanced decline of land near-surface relative humidity to abrupt 4xCO2 in CNRM-CM6-1. *Climate Dynamics, 55*(5), 1613-1629. doi:10.1007/s00382-020-05351-x

Douville, H., & Plazzotta, M. (2017). Midlatitude Summer Drying: An Underestimated Threat in CMIP5 Models? *Geophysical Research Letters, 44*(19), 9967-9975. doi:10.1002/2017GL075353

Douville, H., & Willett, K. M. (2023). A drier than expected future, supported by near-surface relative humidity observations. *Science Advances, 9*(30), eade6253. doi:doi:10.1126/sciadv.ade6253

Dunn, R. J. H., Willett, K. M., Ciavarella, A., & Stott, P. A. (2017). Comparison of land surface humidity between observations and CMIP5 models. *Earth Syst. Dynam., 8*(3), 719-747. doi:10.5194/esd-8-719-2017

Eyring, V., Bony, S., Meehl, G. A., Senior, C. A., Stevens, B., Stouffer, R. J., & Taylor, K. E. (2016). Overview of the Coupled Model Intercomparison Project Phase 6 (CMIP6) experimental design and organization. *Geoscientific Model Development, 9*(5), 1937-1958. doi:10.5194/gmd-9-1937-2016

Fisher, J. B., Melton, F., Middleton, E., Hain, C., Anderson, M., Allen, R., . . . Wood, E. F. (2017). The future of evapotranspiration: Global requirements for ecosystem functioning, carbon and climate feedbacks, agricultural management, and water resources. *Water Resources Research, 53*(4), 2618-2626. doi:10.1002/2016WR020175

Gentine, P., Chhang, A., Rigden, A., & Salvucci, G. (2016). Evaporation estimates using weather station data and boundary layer theory. *Geophysical Research Letters, 43*(22), 11,661-611,670. doi:10.1002/2016gl070819

Held, I. M., & Soden, B. J. (2006). Robust responses of the hydrological cycle to global warming. *Journal of Climate, 19*(21), 5686-5699.

Hersbach, H., Bell, B., Berrisford, P., Hirahara, S., Horányi, A., Muñoz-Sabater, J., . . . Schepers, D. (2020). The ERA5 global reanalysis. *Quarterly Journal of the Royal Meteorological Society, 146*(730), 1999-2049.

Jung, M., Reichstein, M., Ciais, P., Seneviratne, S. I., Sheffield, J., Goulden, M. L., . . . Zhang, K. (2010). Recent decline in the global land evapotranspiration trend due to limited moisture supply. *Nature, 467*(7318), 951-954. doi:10.1038/nature09396

Kim, Y., Garcia, M., Black, T. A., & Johnson, M. (2023). Assessing the complementary role of surface flux equilibrium (SFE) theory and maximum entropy production (MEP) principle in the estimation of actual evapotranspiration. *Journal of Advances in Modeling Earth Systems, 15*(e2022MS003224). doi:10.1029/2022MS003224

Kim, Y., Garcia, M., & Johnson, M. S. (2023). Land-atmosphere coupling constrains increases to potential evaporation in a warming climate: Implications at local and global scales. *Earth's Future, 11*(2), e2022EF002886. doi:10.1029/2022EF002886

Kim, Y., Garcia, M., Morillas, L., Weber, U., Black, T. A., & Johnson, M. S. (2021). Relative humidity gradients as a key constraint on terrestrial water and energy fluxes. *Hydrol. Earth Syst. Sci., 25*(9), 5175-5191. doi:10.5194/hess-25-5175-2021

Knauer, J., El-Madany, T. S., Zaehle, S., & Migliavacca, M. (2018). Bigleaf—An R package for the calculation of physical and physiological ecosystem properties from eddy covariance data. *PLOS ONE, 13*(8), e0201114. doi:10.1371/journal.pone.0201114

Kosaka, Y., Kobayashi, S., Harada, Y., Kobayashi, C., Naoe, H., Yoshimoto, K., . . . Onogi, K. (2024). The JRA-3Q Reanalysis. *Journal of the Meteorological Society of Japan. Ser. II, 102*(1), 49-109. doi:10.2151/jmsj.2024-004

Ma, H.-Y., Klein, S. A., Xie, S., Zhang, C., Tang, S., Tang, Q., . . . Wang, Y.-C. (2018). CAUSES: On the Role of Surface Energy Budget Errors to the Warm Surface Air Temperature Error Over the Central United States. *Journal of Geophysical Research: Atmospheres, 123*(5), 2888-2909. doi:10.1002/2017jd027194

Ma, N., Zhang, Y., & Szilagyi, J. (2024). Water-balance-based evapotranspiration for 56 large river basins: A benchmarking dataset for global terrestrial evapotranspiration modeling. *Journal of Hydrology*, 130607. doi:10.1016/j.jhydrol.2024.130607

McColl, K. A., & Rigden, A. J. (2020). Emergent Simplicity of Continental Evapotranspiration. *Geophysical Research Letters, 47*(6), e2020GL087101. doi:10.1029/2020gl087101

McColl, K. A., Roderick, M. L., Berg, A., & Scheff, J. (2022). The terrestrial water cycle in a warming world. *Nature Climate Change, 12*(7), 604-606. doi:10.1038/s41558-022-01412-7

McColl, K. A., Salvucci, G. D., & Gentine, P. (2019). Surface flux equilibrium theory explains an empirical estimate of water-limited daily evapotranspiration. *Journal of Advances in Modeling Earth Systems, 11*(7), 2036-2049. doi:10.1029/2019ms001685

McColl, K. A., & Tang, L. I. (2024). An Analytic Theory of Near-Surface Relative Humidity over Land. *Journal of Climate, 37*(4), 1213-1230. doi:10.1175/jcli-d-23-0342.1

Milly, P. C. D., Betancourt, J., Falkenmark, M., Hirsch, R. M., Kundzewicz, Z. W., Lettenmaier, D. P., & Stouffer, R. J. (2008). Stationarity Is Dead: Whither Water Management? *Science, 319*(5863), 573-574. doi:10.1126/science.1151915

Milly, P. C. D., & Dunne, K. A. (2016). Potential evapotranspiration and continental drying. *Nature Climate Change, 6*(10), 946-949. doi:10.1038/nclimate3046

Milly, P. C. D., & Dunne, K. A. (2020). Colorado River flow dwindles as warming-driven loss of reflective snow energizes evaporation. *Science, 367*(6483), 1252-1255. doi:10.1126/science.aay9187

O'Gorman, P. A., & Muller, C. J. (2010). How closely do changes in surface and column water vapor follow Clausius–Clapeyron scaling in climate change simulations? *Environmental Research Letters, 5*(2), 025207. doi:10.1088/1748-9326/5/2/025207

Pan, S., Pan, N., Tian, H., Friedlingstein, P., Sitch, S., Shi, H., . . . Running, S. W. (2020). Evaluation of global terrestrial evapotranspiration using state-of-the-art approaches in remote sensing, machine learning and land surface modeling. *Hydrol. Earth Syst. Sci., 24*(3), 1485-1509. doi:10.5194/hess-24-1485-2020

Pastorello, G., Trotta, C., Canfora, E., Chu, H., Christianson, D., Cheah, Y.-W., . . . Papale, D. (2020). The FLUXNET2015 dataset and the ONEFlux processing pipeline for eddy covariance data. *Scientific Data, 7*(1), 225. doi:10.1038/s41597-020-0534-3

Scheff, J., Coats, S., & Laguë, M. M. (2022). Why do the Global Warming Responses of Land-Surface Models and Climatic Dryness Metrics Disagree? *Earth's Future, 10*(8), e2022EF002814. doi:10.1029/2022EF002814

Seltzer, A. M., Blard, P.-H., Sherwood, S. C., & Kageyama, M. (2023). Terrestrial amplification of past, present, and future climate change. *Science Advances, 9*(6), eadf8119. doi:doi:10.1126/sciadv.adf8119

Sherwood, S., & Fu, Q. (2014). A drier future? *Science, 343*(6172), 737-739. doi:10.1126/science.1247620

Simmons, A. J., Willett, K. M., Jones, P. D., Thorne, P. W., & Dee, D. P. (2010). Low-frequency variations in surface atmospheric humidity, temperature, and precipitation: Inferences from reanalyses and monthly gridded observational data sets. *Journal of Geophysical Research: Atmospheres, 115*(D1). doi:10.1029/2009JD012442

Simpson, I. R., McKinnon, K. A., Kennedy, D., Lawrence, D. M., Lehner, F., & Seager, R. (2024). Observed humidity trends in dry regions contradict climate models. *Proceedings of the National Academy of Sciences, 121*(1), e2302480120. doi:doi:10.1073/pnas.2302480120

Twine, T. E., Kustas, W. P., Norman, J. M., Cook, D. R., Houser, P. R., Meyers, T. P., . . . Wesely, M. L. (2000). Correcting eddy-covariance flux underestimates over a grassland. *Agricultural and Forest Meteorology, 103*(3), 279-300. doi:10.1016/S0168-1923(00)00123-4

Vargas Zeppetello, L. R., McColl, K. A., Bernau, J. A., Bowen, B. B., Tang, L. I., Holbrook, N. M., . . . Huybers, P. (2023). Apparent surface conductance sensitivity to vapour pressure deficit in the absence of plants. *Nature Water, 1*(11), 941-951. doi:10.1038/s44221-023-00147-9

Vicente-Serrano, S. M., McVicar, T. R., Miralles, D. G., Yang, Y., & Tomas-Burguera, M. (2020). Unraveling the influence of atmospheric evaporative demand on drought and its response to climate change. *WIREs Climate Change, 11*(2), e632. doi:10.1002/wcc.632

Vicente-Serrano, S. M., Nieto, R., Gimeno, L., Azorin-Molina, C., Drumond, A., El Kenawy, A., . . . Peña-Gallardo, M. (2018). Recent changes of relative humidity: regional connections with land and ocean processes. *Earth Syst. Dynam., 9*(2), 915-937. doi:10.5194/esd-9-915-2018

Wang, L., Jiao, W., MacBean, N., Rulli, M. C., Manzoni, S., Vico, G., & D'Odorico, P. (2022). Dryland productivity under a changing climate. *Nature Climate Change, 12*(11), 981-994. doi:10.1038/s41558-022-01499-y

Willett, K., Dunn, R., Thorne, P., Bell, S., De Podesta, M., Parker, D., . . . Williams Jr, C. (2014). HadISDH land surface multi-variable humidity and temperature record for climate monitoring. *Climate of the Past, 10*(6), 1983–2006.

Xu, W., Xia, X., Piao, S., Wu, D., Li, W., Yang, S., & Yuan, W. (2024). Weakened Increase in Global Near-Surface Water Vapor Pressure During the Last 20 Years. *Geophysical Research Letters, 51*(2), e2023GL107909. doi:10.1029/2023GL107909

Yang, Y., Roderick, M. L., Guo, H., Miralles, D. G., Zhang, L., Fatichi, S., . . . Yang, D. (2023). Evapotranspiration on a greening Earth. *Nature Reviews Earth & Environment, 4*(9), 626-641. doi:10.1038/s43017-023-00464-3

Zaitchik, B. F., Rodell, M., Biasutti, M., & Seneviratne, S. I. (2023). Wetting and drying trends under climate change. *Nature Water, 1*(6), 502-513. doi:10.1038/s44221-023-00073-w

Zhou, W., Leung, L. R., & Lu, J. (2023). The Role of Interactive Soil Moisture in Land Drying Under Anthropogenic Warming. *Geophysical Research Letters, 50*(19), e2023GL105308. doi:10.1029/2023GL105308

Acknowledgments

We are grateful for FLUXNET2015 site PIs, ERA5 and JRA-3Q reanalysis developing groups, and the CMIP6 climate modelling groups, and appreciate the efforts of data providers for producing and making available these datasets. We express our thanks to the development of the ocean-influence theory (by M. Byrne, P. O'Gorman, R. Chadwick, P. Good, K. Willett, and others) that inspired our theoretical framework.

Funding: We acknowledge the support of the Canadian Space Agency (CSA) Grant 21SUESIELH.

Author contributions:

Conceptualization: YK, MSJ
Methodology: YK, MSJ
Investigation: YK, MSJ
Visualization: YK
Supervision: MSJ
Writing—original draft: YK
Writing—review & editing: MSJ

Competing interests: Authors declare that they have no competing interests.

Data and materials availability: All data used in the main text and the supplementary materials are publicly available. The FLUXNET2015 dataset can be obtained from the FLUXNET data portal (https://fluxnet.org/data/fluxnet2015-dataset/), the ERA5 reanalysis data can be obtained from CDS of ECMWF (https://doi.org/10.24381/cds.f17050d7), the JRA-3Q reanalysis data can be obtained from DIAS (https://doi.org/10.20783/DIAS.645), the CMIP6 models outputs can be obtained from CDS of the ECMWF (https://doi.org/10.24381/cds.c866074c).
The code used for these analyses will be publicly available prior to publication.

Supplementary Materials

Supplementary Materials file includes:
Figs. S1 to S2
Tables S1

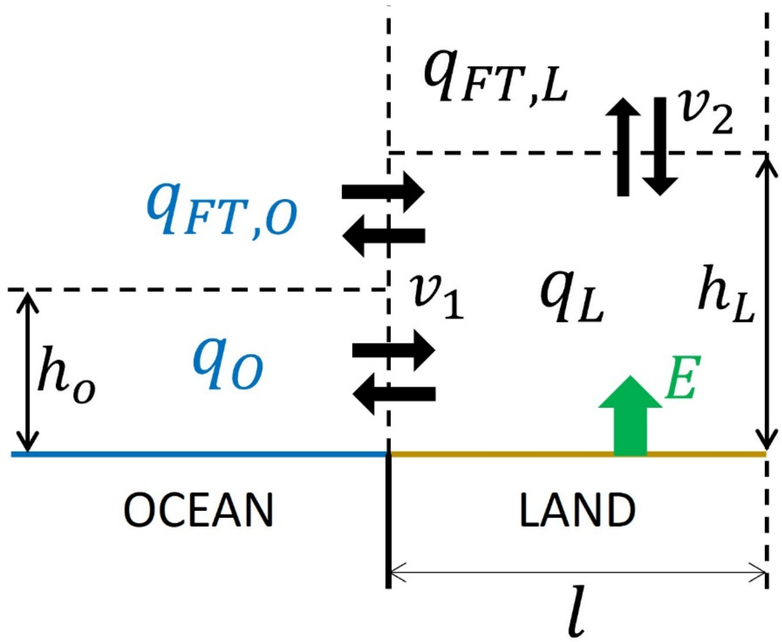

Fig. S1. Schematic representation of the parsimonious atmospheric boundary layer box, adapted from Byrne & O'Gorman (2016). In this illustration, E represents terrestrial evapotranspiration, h is the boundary layer height, l is the length of the land, q is specific humidity, v_1 is horizontal mixing velocity, and v_2 is vertical mixing velocity. The subscripts O and L respectively denote ocean and land, while the subscript FT indicates the free troposphere immediately above the land and ocean boundary layers.

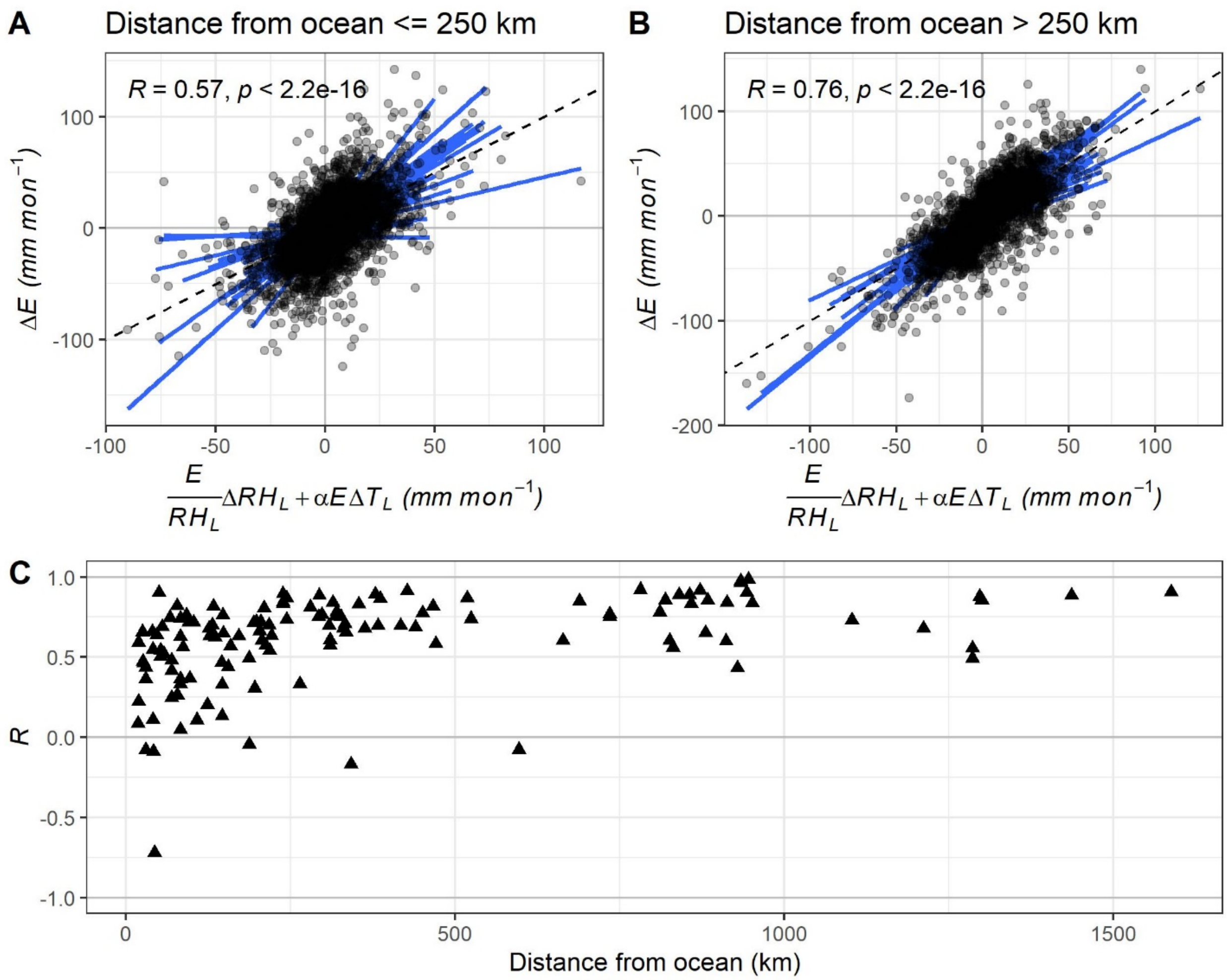

Fig. S2. Similar to Fig. 2 but using energy balance corrected *E* employing Bowen ratio preservation method (Pastorello et al., 2020; Twine et al., 2000).

Table S1. List of CMIP6 models used in this study

Model	Modeling Center
ACCESS-CM2	CSIRO-ARCCSS (Commonwealth Scientific and Industrial Research Organisation, Australian Research Council Centre of Excellence for Climate System Science)
AWI-CM-1-1-MR	AWI (Alfred Wegener Institute)
CanESM5-CanOE	CCCMA (Canadian Centre for Climate Modelling and Analysis)
CESM2	NCAR (National Center for Atmospheric Research)
CMCC-CM2-SR5	CMCC (Centro Euro-Mediterraneo per I Cambiamenti Climatici)
CMCC-ESM2	
CNRM-CM6-1	CNRM-CERFACS (National Center for Meteorological Research, Météo-France and CNRS laboratory, Climate Modeling and Global change)
CNRM-CM6-1-HR	
CNRM-ESM2-1	
E3SM-1-1	E3SM-Project RUBISCO (Energy Exascale Earth System Model, Reducing Uncertainty in Biogeochemical Interactions through Synthesis and COmputation)
FGOALS-f3-L	CAS (Chinese Academy of Sciences)
FGOALS-g3	
FIO-ESM-2-0	FIO-QLNM (First Institute of Oceanography (FIO) and Qingdao National Laboratory for Marine Science and Technology (QNLM))
GFDL-ESM4	NOAA-GFDL (National Oceanic and Atmospheric Administration, Geophysical Fluid Dynamics Laboratory)
HadGEM3-GC31-LL	MOHC (Met Office Hadley Centre)
HadGEM3-GC31-MM	
INM-CM4-8	INM (Institute of Numerical Mathematics)
INM-CM5-0	
IPSL-CM6A-LR	IPSL (Institut Pierre-Simon Laplace)
KACE-1-0-G	NIMS-KMA (National Institute of Meteorological Sciences/Korea Met. Administration)
MIROC6	MIROC (Atmosphere and Ocean Research Institute (AORI), Centre for Climate System Research - National Institute for Environmental Studies (CCSR-NIES) and Atmosphere and Ocean Research Institute (AORI))
MIROC-ES2L	
MPI-ESM1-2-LR	MPI-M AWI (Max Planck Institute for Meteorology (MPI-M), AWI (Alfred Wegener Institute))
MRI-ESM2-0	MRI (Meteorological Research Institute, Japan)
NorESM2-MM	NCC (Norwegian Climate Centre)
TaiESM1	AS-RCEC (Research Center for Environmental Changes)
UKESM1-0-LL	MOHC, NERC, NIMS-KMA, NIWA (Met Office Hadley Centre, Natural Environmental Research Council, National Institute of Meteorological Science / Korean Meteorological Administration (NIMS-KMA), National Institute of Weather and Atmospheric Research (NIWA))